



Welding fume nanoparticles from solid and flux-cored wires: Solubility, toxicity, and role of fluorides

Y.S. Hedberg^{a,b,c,*}, Z. Wei^a, S. McCarrick^d, V. Romanovski^{a,e,f}, J. Theodore^a, E.M. Westin^g, R. Wagner^h, K.-A. Perssonⁱ, H.L. Karlsson^d, I. Odnevall Wallinder^{a,j,k,**}

^a KTH Royal Institute of Technology, Department of Chemistry, Division of Surface and Corrosion Science, 10044 Stockholm, Sweden

^b Department of Chemistry, The University of Western Ontario, London, Ontario N6A 3K7, Canada

^c Surface Science Western, The University of Western Ontario, London, Ontario N6G 0J3, Canada

^d Institute of Environmental Medicine, Karolinska Institutet, 171 77 Stockholm, Sweden

^e Center of Functional Nano-Ceramics, National University of Science and Technology "MISIS", 119049 Moscow, Russia

^f Institute of General and Inorganic Chemistry, National Academy of Sciences of Belarus, 220072 Minsk, Belarus

^g voestalpine Böhler Welding Group GmbH, Böhler-Welding-Str. 1, 8605 Kapfenberg, Austria

^h Linde GmbH/UniBw Munich, Germany

ⁱ Swerim AB, SE-164 07 Kista, Sweden

^j AIMES - Center for the Advancement of Integrated Medical and Engineering Sciences at Karolinska Institutet and KTH Royal Institute of Technology, Stockholm, Sweden

^k Department of Neuroscience, Karolinska Institutet, SE-171 77 Stockholm, Sweden

ARTICLE INFO

Editor: Dr. S. Nan

Keywords:

Metal release

Solubility

XRD

XPS

Cyclic voltammetry

FTIR

TEM

Cytotoxicity

Genotoxicity

Welding

ABSTRACT

Welding fume particles are hazardous. Their toxicity likely depends on their composition and reactivity. This study aimed at exploring the role of sodium or other fluorides (NaF), which are intentionally added to flux-cored wire electrodes for stainless steel welding, on the solubility (in phosphate buffered saline) and toxicity of the generated welding fume particles. A multi-analytical particle characterization approach along with in-vitro cell assays was undertaken. The release of Cr(VI) and Mn from the particles was tested as a function of fluoride solution concentration. The welding fume particles containing NaF released significantly higher amounts of Cr (VI) compared with solid wire reference fumes, which was associated with increased cytotoxicity and genotoxicity in-vitro. No crystalline Na or potassium (K) containing chromates were observed. Cr(VI) was incorporated in an amorphous mixed oxide. Solution-added fluorides did not increase the solubility of Cr(VI), but contributed to a reduced Mn release from both solid and flux-cored wire fume particles and the reduction of Cr (VI) release from solid wire fume particles. Chemical speciation modeling suggested that metal fluoride complexes were not formed. The presence of NaF in the welding electrodes did not have any direct, but possibly an indirect, role in the Cr(VI) solubility of welding fumes.

1. Introduction

Welders without sufficient protection equipment are exposed to potentially hazardous welding fumes. Despite significant efforts to improve occupational health safety, exposure to welding fume remains a serious problem even in developed countries with a long history to improve work environment conditions. For example, a recent report commissioned by the Swedish Work Environment Authority (Andersson et al., 2019) estimates 71 death cases annually (based on 2016 data) in Sweden that could be directly related to welding fume (considering

ischemic heart disease and lung cancer as death causes). This is more than the total annual death cases related to work accidents in all occupations in Sweden. In the UK, 152 deaths (lung cancer only) are estimated annually due to occupational exposure to welding fume (Rushton et al., 2012).

Exposure to welding fume is associated with an increased risk of developing lung cancer (IARC, 2018; Honaryar et al., 2019), cardiovascular diseases (Ellingsen et al., 2019; Ibfelt et al., 2010), and a number of lung and airway diseases (Antonini et al., 2003; Coggon and Palmer, 2016; Zeidler-Erdely et al., 2012), partially due to suppression

* Correspondence to: The University of Western Ontario, Department of Chemistry, London, Ontario N6A 3K7, Canada.

** Correspondence to: KTH Royal Institute of Technology, Department of Chemistry, Division of Surface and Corrosion Science, 10044 Stockholm, Sweden.

E-mail addresses: yhedberg@uwo.ca (Y.S. Hedberg), ingero@kth.se (I. Odnevall Wallinder).

<https://doi.org/10.1016/j.jhazmat.2021.125273>

Received 13 September 2020; Received in revised form 21 January 2021; Accepted 27 January 2021

Available online 5 February 2021

0304-3894/© 2021 The Author(s). Published by Elsevier B.V. This is an open access article under the CC BY license (<http://creativecommons.org/licenses/by/4.0/>).

of the immune system (Zeidler-Erdelyi et al., 2012; Knobloch et al., 2020). Welding fume, without any distinction of the material or welding method, has been classified as Group 1 carcinogenic to humans by the International Agency for Research on Cancer (IARC) (IARC, 2018). It has been shown that there is an increased risk independent of type of welding fume (IARC, 2018; Honaryar et al., 2019). Exposure to small particles, including welding fume, is also in general associated with acute myocardial infarction and other ischemic heart disease (Wiebert et al., 2012; Mocevic et al., 2015; Sjögren et al., 2002). Further, air pollution, including particulate matter which can reach the brain, has been linked to central nervous system diseases such as Alzheimer's disease, Parkinson's disease, and stroke (Block and Calderón-Garcidueñas, 2009). Welding fume consists of both potentially hazardous gases and particles, which often are nano-sized (Flores, 2018).

The authors have shown considerable variations in in-vitro toxicity (cytotoxicity, generation of reactive oxygen species, and genotoxicity) that correlate with the released amount of hexavalent chromium [Cr(VI)] and manganese (Mn) from stainless steel welding fume particles at physiological pH (McCarrick et al., 2019). These findings are in line with epidemiological evidence showing an increased lung cancer risk if exposed to high ($\geq 1.8 \text{ mg/m}^3$) amounts of welding fume and high ($\geq 1.4 \text{ }\mu\text{g/m}^3$) amounts of Cr(VI) in the work environment (Kendzia et al., 2020). Mn in, or released from, welding fume can cause neurotoxic effects (Taube, 2013). From an exposure point of view, national occupational exposure limits are often exceeded for Mn (Hanley et al., 2017; Jeong et al., 2016; Hedmer et al., 2014). In-vitro and in-vivo studies have shown that welding fumes from stainless steels containing nickel (Ni) and chromium (Cr), which under certain circumstances contains Cr(VI), are significantly more toxic compared to fumes generated from welding mild steel (Antonini et al., 2005, 1999; Leonard et al., 2010; Olgun et al., 2020; Shoeb et al., 2017b, 2017a). However, long-term effects (lung tumor promotions) were in an in-vivo study more strongly associated with less soluble metal compounds in model metal oxide particles, in particular iron (Fe) oxides at physiological pH (Falcone et al., 2018).

Gas metal arc welding (GMAW) and flux-cored arc welding (FCAW) are, due to high-productivity, among the most common welding methods (Flores, 2018; Praveen et al., 2005). These processes result in higher amounts of airborne ultrafine particles as compared to other welding methods, such as tungsten-inert gas welding (Gomes et al., 2012b). In GMAW and FCAW, an electric arc is formed between a consumable wire (electrode or filler material) and the base metal such as stainless steel under the protection of a shielding gas. Solid wire and flux-cored wire (FCW) electrodes are the electrodes for GMAW and FCAW. FCW forms a protective slag on the weld. FCW electrodes consist of a sheath metal filled with a flux powder. The flux contains different salts (often fluorides), metals, and minerals (metal oxides) of widely varying compositions for different applications (Flores, 2018; Guo et al., 2019; Westin et al., 2016). The amount of fluoride salts in FCW depends on the type of the FCW electrode, and typical fluoride salts are sodium fluoride (NaF), calcium difluoride (CaF_2), or perovskite fluoride KCaF_3 (Flores, 2018). Although the amount and composition of the welding fume particles depend on several welding parameters such as melting rate, potential, current, arc mode (e.g. spray arc), filler material feed rate, and shielding gas, the main factor that influences the solubility and composition of the welding fume particles is the composition of the filler material (electrode) (Flores, 2018; McCarrick et al., 2019; Mei et al., 2018). The flux consists of at least a dozen different raw materials and works in symbiosis with the strip composition, thickness, and various coatings for feedability. All of these parameters have individual, antagonistic, or synergistic influences on arc stability, fluidity and viscosity, slag formation, element loss, and weldability.

Since the release of Cr(VI) and Mn from welding fume particles are important processes that govern acute toxic effects, inflammatory markers, and genotoxicity, and since their solubility varies largely as a

function of welding electrode and welding parameters (McCarrick et al., 2019; Antonini et al., 2004), it is crucial to understand the underlying chemical and physical reasons for Cr(VI) and Mn solubility in welding fume under physiologically relevant conditions. An evident correlation has been observed between fluoride salts [often containing sodium (Na) or potassium (K)] and soluble Cr(VI) in welding fume of stainless steel welded with certain FCW electrodes (Mei et al., 2018; Tandon et al., 1985; Flores, 2016). It is however unclear, if Na or K contribute to the formation of easily soluble chromate compounds (Flores, 2018; Tandon et al., 1985), whether fluoride ions could play a role, and/or whether other factors need to be considered. Knowledge of the underlying physicochemical mechanism of the formation and stabilization of soluble Cr(VI) in these welding fume particles would enable reduction of these hazards by means of appropriate engineering and chemical measures.

The aim of this study was therefore to explore the roles of NaF and welding fume composition of welding fume generated by welding stainless steel with a flux-cored wire electrode on the release and soluble fraction of Cr, Cr(VI), Mn, Ni, and Fe, cytotoxicity, and genotoxicity.

2. Materials and methods

2.1. Materials and welding method

The base material was 5 mm austenitic 1.4307/AISI 304 L (denoted 304 L in the following) and 6 mm lean duplex 1.4162/UNS S32101 (denoted 2101). The composition of the base metals is given in Table A1 (supplementary material). Welding was performed using either solid wire electrodes (for samples S1 and S2) or FCW electrodes (for samples F1 and F2). The FCW electrode for F1 was optimized for a fast-freezing slag and the FCW electrode for F2 for a slow-freezing slag (for welding in flat position). The chemical composition of the filler materials used and the classification in accordance with the American Welding Society (AWS) standards AWS A5.9 and A5.22 are given in Table 1. Please note that the wire manufacturers do not provide the formulation of the flux in the FCW products as the combination of oxides and fluoride salts affect the weldability and formation of slag rather than the chemical composition. All wires had a 1.2 mm diameter and were delivered on 15 kg wire baskets.

Welding was performed bead-on-plate by experienced welding operators using the spray arc mode (high current resulting in high melting rates). The welding parameters are presented in Table 2. For FCW, argon with 18% CO_2 , is the optimum shielding gas for arc stability, sidewall fusion, and mechanical properties. The slag cover protects the melt from oxidation and only a minor increase in carbon uptake takes place during the welding process. When welding the gas shielded solid wires, however, it is necessary to avoid significant uptake of carbon and oxygen in the weld metal. Argon with 2% CO_2 offers good arc stability, while the corrosion resistance and mechanical properties are retained.

Collected fume particles were brushed from the cellulose filters, which were used for collection, directly after welding and delivered for analysis in sealed glass vessels. The vessels were kept in a desiccator (< 10% relative humidity) at room temperature prior to and in between the different measurements.

2.2. Electron microscopy

Particle morphology and elemental composition were investigated by means of transmission electron microscopy (TEM) with a JEM-2100F instrument equipped with energy dispersive X-ray spectroscopy (EDS, EDAX Genesis XM 460 system). The operating voltage was 80–200 kV and the lateral resolution was $\geq 0.14 \text{ nm}$. Images were captured in both secondary electron (SE) and back scatter electron (BSE) mode, as well as in STEM mode using the Gatan Ultrascan 100 16 MP camera. The preparation of the fume samples for TEM analysis included the preparation of a suspension of particles in ethanol, ultrasonic treatment for 5

Table 1

Chemical composition of the individual heat number of the iron-based filler metals in wt%. The solid wires S1 and S2 show the wire analysis and the flux-cored wires F1 and F2 the analysis of the all-weld metal with Ar + 18% CO₂ as shielding gas.

Type	C	Si	Mn	P	S	Fe	Cr	Ni	Mo	Cu	N	
S1	ER308L	0.020	0.76	1.7	0.018	0.004	67	20	11	0.10	0.10	0.046
S2	ER2307	0.020	0.54	0.80	0.022	0.001	67	23	7.4	0.20	0.20	0.12
F1	E308LT1	0.026	0.71	1.3	0.020	0.004	68	20	10	0.04	0.10	0.017
F2	E2307T0	0.029	0.68	1.3	0.020	0.006	64	25	9.0	0.38	0.04	0.15

Table 2

Welding parameters. The polarity was DC+, the shielding gas flow rate 18–20 L/min and the wire stick-out 18–20 mm.

Wire	Base metal	Shielding gas	Welding speed (m/min)	Wire feed speed (m/min)	Voltage (V)	Arc time (s)	Current (A)
S1	304 L	Ar + 2% CO ₂	0.32	7.4	30	411	270
S2	2101	Ar + 2% CO ₂	0.36	10.5	30	230	260
F1	304 L	Ar + 18% CO ₂	0.39	10.5	29	142	260
F2	2101	Ar + 18% CO ₂	0.38	10.5	29	145	260

min, and centrifugation for 5 min at 5000 rpm. A drop of the supernatant was then pipetted on the TEM copper grid (covered with carbon) and dried at ambient conditions. Image processing and particle size distribution calculations were performed by means of the ImageJ software for 247–682 independent particles for each sample.

Morphological information was obtained by using a Hitachi SU8230 Regulus Ultra High-Resolution Field Emission SEM (FE-SEM) equipped with EDS. The images were captured in both SE mode and BSE mode with a setting of 15 kV. EDS was performed as area analysis on nanoparticle aggregates and additionally as spot analysis on micrometer-sized spherical particles and nanoparticle aggregates in their vicinity. Image processing and particle size distribution calculations were also performed for 162–270 independent particles for each sample based on the SEM images.

2.3. X-ray diffraction (XRD)

The phase composition and crystal structure of the fume samples were characterized by XRD using a Bruker D8 ADVANCE diffractometer with a rotating cobalt radiation. The reference data was used from the PDF2 database. Rietveld refinements were conducted with the software HighScore Plus. The pseudo-Voigt function was used for the peak profile refinement. The average crystal size (d , in nm) in the welding fume particles was calculated by the Scherrer formula $d = K\lambda/\beta\cos\theta$, where the dimensionless particle shape factor (Scherrer's constant) $K = 0.94$ for cubic crystals, the wavelength of X-ray radiation (of the Co source) $\lambda = 0.1788965$ nm (cobalt line), β is the width at half the maximum peak intensity, and θ is the angle of diffraction (Bragg angle), here chosen for the highest intensity peak (Alexander and Klug, 1950).

2.4. X-ray photoelectron spectroscopy (XPS)

The outermost surface (5–10 nm) composition was determined by means of XPS using an UltraDLD spectrometer, Kratos Analytical Manchester, UK, with a monochromatic Al K α X-ray source (150 W). The fume particles were fixed on adhesive copper tape. Wide spectra and detailed spectra (pass energy of 20 eV) for Fe 2p, Cr 2p, Ni 2p, Mn 2p, Si 2p, K 2p, Bi 4f, Na 1s, F 1s, O 1s, and C 1s (as energy reference at 285.0 eV) were run for two different locations for each sample. Quantitative information was obtained by using linear background corrections and peak fitting based on the Gaussian-Lorentzian function.

2.5. Fourier-transform infrared spectroscopy (FTIR)

An infrared (IR) Fourier spectrometer NEXUS E.S.P. (Thermo Scientific, USA) was used to acquire 32 spectra with 4 cm⁻¹ resolution in the transmission mode of the welding particles mixed with potassium

bromide (KBr) pressed into a pellet (2 wt% welding fume particles, 98 wt % KBr). The background was measured prior to each measurement and subtracted.

2.6. Cyclic voltammetry (CV)

The welding fume samples were immobilized on a paraffin-impregnated graphite electrode (PIGE) as working electrode for CV measurements in 8 M NaOH (pH 13) with a platinum wire as counter electrode, and an Ag/AgCl (sat. KCl) as reference electrode. The potential was swept cathodically from the open-circuit potential to -1.4 V vs. Ag/AgCl sat. KCl and anodically to 0.2 V, or vice versa, in order to investigate solid-solid transformation peaks corresponding to reduction or oxidation of electroactive species in the surface oxide of the welding fume particles. Detailed methodological information is given in previously published studies (Mei et al., 2018; Cha et al., 2016).

2.7. Digestion for total metal content analysis

5 ± 0.5 mg of the welding fume samples was weighed using a microbalance with 2 µg readability (XP26 DeltaRange®, METTLER TOLEDO, Sweden), documented for each sample. 20 mL of diluted aqua regia (2.5 vol% HCl and 6.5 vol% HNO₃) was added before sonicated in an ultrasonic bath for 2 h. This resulted in a final solution temperature of 60–70 °C. The digested sample was then kept in the diluted aqua regia for at least 24 h prior to solution analysis (Section 2.10). Triplicate samples and one background sample (blank), without welding fume, were prepared for each welding fume sample. Ultrapure water (18.2 MΩ cm, Millipore, Sweden) was used as solvent for all solutions.

2.8. Release testing in phosphate buffered saline (PBS) with and without addition of NaF

5 ± 0.5 mg of the welding fume samples was weighed into acid-cleaned dry Nalgene® polypropylene vessels, with the exact weight recorded. 50 mL of PBS (8.77 g/L NaCl, 1.28 g/L Na₂HPO₄, 1.36 g/L KH₂PO₄, adjusted with 50% NaOH to pH 7.2–7.4) were then added and the closed vessels were exposed for 24 h at 37 °C in darkness in an incubator (Edmund Bühler GmbH TH30, Bodelshausen, Germany) with bi-linear agitation (22 cycles/min, 12° inclination). After exposure, the pH of each sample (triplicate samples and one blank sample) was measured and the solutions filtered (GE Healthcare Whatman, 25 mm diameter, 0.02 µm inorganic syringe membrane filter anotop™) and frozen prior to further analysis (Section 2.10).

The same procedure was followed for different added amounts of NaF (analytical grade) during exposure in PBS. 0, 1, 5, 10, and 50 mg F/L (from NaF) in PBS was used to investigate the effect of fluorides on the

release of metals from the welding fume samples S2 and F2.

The effect of fluoride adsorption on the release of Cr(VI) was also attempted to be investigated by a double-step exposure. The welding fume sample S1 was exposed to PBS containing fluorides (50 mg F/L) in a centrifuge tube followed by centrifugation at 3000 rcf. After 10 min the solution was decanted, and fluoride-free PBS was added.

2.9. Cr(VI) extraction in carbonate solution

Extraction at alkaline conditions according to the ISO standards (ISO, 2017a, 2005) was also conducted in order to compare the Cr(VI) solubility tests in PBS with industrial methods. 10 mg of the welding fume sample was extracted for Cr(VI) by adding 2.5 mL of a leaching solution (20 g/L NaOH and 30 g/L Na₂CO₃) and 5 mL of ultrapure water, resulting in a final pH of 12.6. This solution was then heated near the boiling point (until visible bubbles) for 30 min in an acid-cleaned glass vessel covered with a microscope cover glass. After that procedure, the solution was filtered using a paper filter (VWR, qualitative filter paper, 413, particle retention 5–13 µm, European Cat. No 516-0816), and filled up to 25 mL with ultrapure water prior to any further dilution with ultrapure water and analysis for Cr(VI) by means of spectrophotometry (Section 2.10).

2.10. Analysis of metals in solution and Cr(VI) in solution

Flame atomic absorption spectroscopy (AAS) was employed to analyze total concentrations of Cr, Ni, Fe, and Mn in the solution samples (AAAnalyst 800, Perkin Elmer, Waltham, MA). Prior to analysis, the unfrozen solution samples were acidified with ultrapure HNO₃ to a pH < 2. Ultrapure water and 3–4 standard solution samples prepared in 1% HNO₃ were used for calibration. One of these standard solution samples was checked regularly (every 5th sample) to detect deviations from the calibration curve and, if necessary, recalibrate. The detection limits, as estimated from three times the average standard deviations of the blank samples, were 0.02 mg Cr/L, 0.05 mg Fe/L, 0.04 mg Mn/L, and 0.03 mg Ni/L.

960 µL of the unfrozen PBS solution samples were mixed with 20 µL of diphenylcarbazide (DPC) solution and 20 µL phosphoric acid (70%). The DPC solution, composed of 1.0 g 1,5-diphenylcarbazide in 100 mL acetone, was acidified with one drop of glacial ultrapure acetic acid. The concentration of Cr(VI) was determined at 540 nm using a UV–vis spectrophotometer (Jenway 6300) following the procedure described in ISO (2017b). The calibration was based on PBS blank samples with additions of 0, 125, 247.5, 495 and 990 µg/L Cr(VI). The calibration curves were linear ($R^2 \geq 0.9997$). The limit of detection, as based on three times the highest standard deviation of the blank samples, was $\leq 60 \mu\text{g/L}$.

2.11. In-vitro toxicity assays

2.11.1. Cell culture and reagents

Human bronchial epithelial cells (HBEC3-kt) were cultured at serum-free conditions in 50% LHC-9 (Laboratory of Human Carcinogenesis-9) medium and 50% RPMI (Roswell Park Memorial Institute) medium supplemented with 1% penicillin-streptomycin (PEST, Gibco) and 1% L-glutamine. Prior to sub-culturing, flasks or plates were pre-coated with 0.01% collagen (Type I, PureColVR, Advanced BioMatrix). Cells were seeded 24 h prior to exposure for each experiment.

2.11.2. Preparation of fume (nano)particles for cell exposure

The welding fume particles were weighed and suspended in ultrapure water in a glass tube at a concentration of 1 mg/mL, followed by sonication in water bath for 2 × 10 min with vortexing prior, in between, and after. Immediately prior to exposure, the particle suspensions were further diluted to desired concentrations in HBEC cell medium. Fresh suspensions were prepared for every experiment.

2.11.3. Cytotoxicity (Alamar blue assay)

HBEC cells were seeded at 1×10^4 cells/well in transparent 96 well plates following exposure to fume particles in HBEC cell medium for 24 h in triplicates. Alamar blue assay was performed as previously described by the authors (Di Bucchianico et al., 2017). Briefly, following exposure, the medium was removed and replaced with 10% Alamar blue reagent in fresh medium and the plate was further incubated for 2 h. The fluorescence was measured using a Tecan Infinite F200 plate reader (Tecan Trading 125 AG, Mannedorf, Switzerland) at 485 nm excitation and 590 nm emission. The average fluorescence intensity for the triplicate in the negative control was set to 100% viability and the mean fluorescence values of the exposed wells were further normalized to this value and calculated as % viability. The results were then expressed as % cytotoxicity calculated by 100 minus % viability. A control experiment with up to 20 µg F/mL (from NaF) without welding fume particles was conducted in parallel. 20 µg F/mL corresponds to the approximate F content (20 wt%) observed in 100 µg/mL welding particles (the highest particle dose tested).

2.11.4. Genotoxicity (comet assay)

Prior to exposure of the welding fume particles, HBEC cells were seeded at 5×10^4 cells in 24 well plates for 3 h. The alkaline version of the comet assay was performed as previously described (Gluga et al., 2014). Subsequent to electrophoresis, the slides were neutralized, dried and stained with 1:10 000 dilution of SYBR Green in TAE buffer for 15 min and scored using a fluorescence microscope (Leica DMLB, Germany) with Comet assay IV software (Perceptive Instruments, Suffolk, UK). 50 cells were scored in duplicate for each sample.

2.12. Joint expert speciation system

The joint expert speciation system (May, 2015) was used to model the chemical speciation of Cr, Mn, Ni, and Fe in PBS and of Cr and Mn in PBS in the presence of 1–50 mg F/L. 25 °C was set as the temperature since the database is most reliable at that temperature. Other input values were pH 7.3, atmospheric pressure, and the calculated ionic strength of the system (180 mM). Solids were allowed to precipitate (which was investigated). The input values for the metals were 19.2 µM Cr³⁺ (1 mg/L), 9.1 µM Mn²⁺ (0.5 mg/L), 3.4 µM Ni²⁺ (0.2 mg/L), 17.9 µM Fe³⁺ (1 mg/L) based on the highest observed aqueous concentrations in PBS and the metal content in the welding fume particles. Other input values were 0.168 M Na⁺, 0.0099 M K⁺, 0.0189 M PO₄³⁻, and 0.15 M Cl⁻. The redox potential was investigated for two conditions: pe 5 and pe 10, which correspond to normal and oxidative conditions in water at pH 7.3. Effects of fluoride concentrations were investigated at 0, 1, 5, 10, and 50 mg F/L.

2.13. Statistical methods

For in-vitro toxicity assays, one-way analysis of variance followed by Dunnett's post hoc test was used to test for significance between exposures and control ($P < 0.05$) using GraphPad Prism 5.02 statistical software (GraphPad Inc., La Jolla, CA). Results are expressed as mean values ± standard deviation (SD) of at least three independent experiments ($n = 3$). For other differences, a student's *t*-test of unpaired data with unequal variance (KaleidaGraph version 4.0, Synergy software, Reading, PA) was used, also with $P < 0.05$ counted as a statistically significant difference. Further details are reported elsewhere (McCarrick et al., 2019).

3. Results and discussion

3.1. Welding fume particle characterization

3.1.1. Electron microscopy and XRD

The high-resolution SEM images (Fig. 1) and TEM images (Fig. A1,

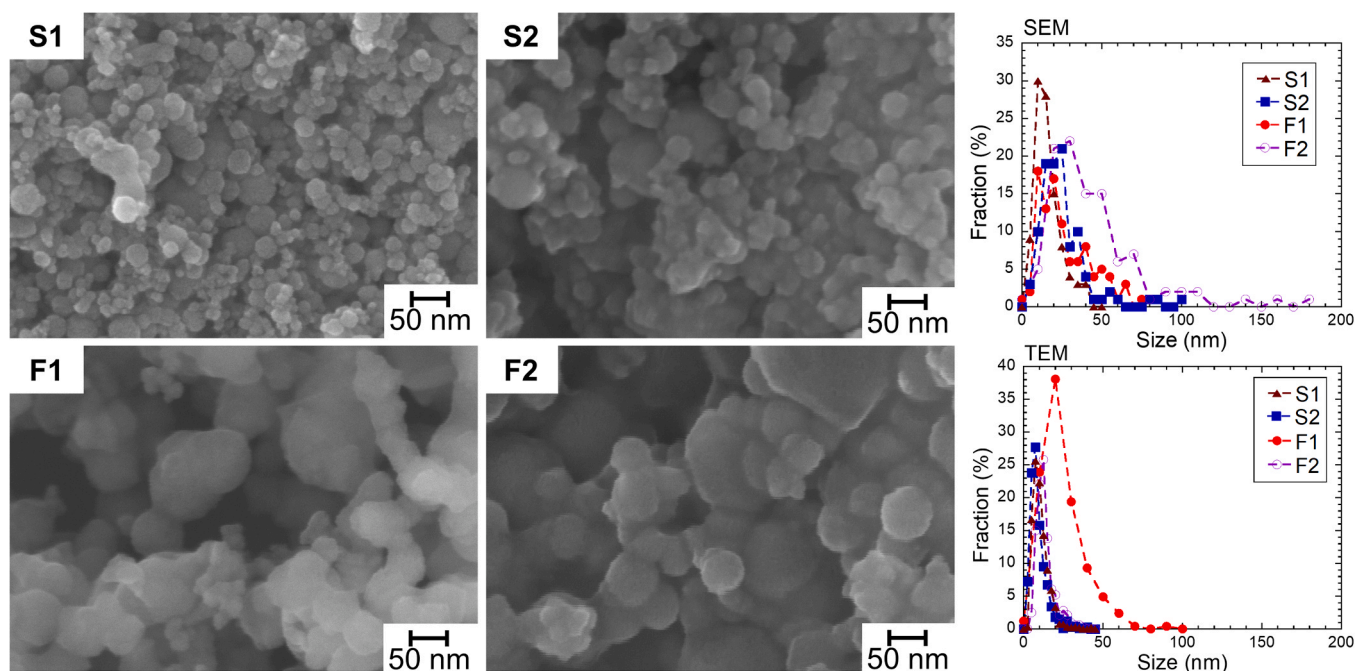


Fig. 1. SEM images (SE mode) at high magnification of the welding fume samples (Solid wire: S1, S2 and flux core wire: F1 and F2) showing the nano-sized particles originating from vapor. Particle size distribution (by number, based on TEM images, see Fig. A1, and based on SEM images) for the welding fume samples S1-S2 and F1-F2. The dotted lines are only guides for the eye.

supplementary material) revealed a primary particle size distribution in the nanometer range for all samples, ranging from 3 to 180 nm, with mean diameters of 11–47 nm (Table A2 and Fig. A1). All particle size histograms were unimodal, with a tail towards larger sizes (Fig. 1).

Overview SEM images shown in Fig. A2 (supplementary material) revealed the majority of the welding fume particles to be aggregated nanoparticles. This is in agreement with literature findings (Flores, 2018; McCarrick et al., 2019; Gomes et al., 2012b, 2012a; Mei et al., 2018) and is a result of solidification (and oxidation) processes of the metal vapor (Flores, 2018). In agreement with previous studies (McCarrick et al., 2019; Mei et al., 2018), spherical micrometer-sized particles were also present showing visible dendrites originating from the solidification of the molten phase (Flores, 2018). Examples of these particles are shown in Fig. 2. These particles seemed to be mainly

metallic, while the nanoparticles had a lower atomic number on average, probably due to oxides, Fig. A3 (supplementary material). The composition of the micrometer-sized spherical particles was similar to what was expected from the base metal (Fig. A4), and surrounding nanoparticles were enriched in oxygen (Fig. A4). The nanoparticle aggregates for samples F1-F2 were significantly enriched in Na, K, and F, and depleted in the main alloying elements. This was most pronounced for sample F2, as judged from the EDS results shown in Table A3. Na and K may originate from fluorides that were intentionally added to the FCW for controlled fluidity, viscosity, and arc stabilization during the welding process. Another origin may be water glass, such as sodium and potassium silicates, that together with water act as binder during flux agglomeration. This water is evaporated by controlled drying in a furnace. Detected titanium possibly originated from rutile TiO_2 used for slag formation in flux-cored wires.

The d-spacing values of 0.489, 0.255, 0.241, 0.232 and 0.148 nm shown in Fig. 3 for the S1, S2, F1, and F2 samples, respectively, correspond to the peaks at 21.10, 41.26, 43.5, 45.43 and 73.94 2-theta in the XRD pattern (Fig. 4). The main diffraction peaks were assigned to a magnetite type phase of X_3O_4 with $\text{X} = \text{Fe}, \text{Cr}, \text{Mn}, \text{and/or Ni}$ for the solid wire fume particles, and to the same phase and NaF in the case of the FCW fume particles (Fig. 4 and Table A4). This is in agreement with literature observations (Flores, 2018; Sowards et al., 2008, 2010; Moroni and Viti, 2009). The content of NaF was significantly larger in sample F2 as compared to F1 (Table A4).

Both amorphous and crystalline phases were observed by high-resolution TEM.

3.1.2. XPS

In agreement with previous studies (McCarrick et al., 2019; Mei et al., 2018) and the EDS results (Table A3), the main alloying elements (Fe, Cr, Mn) were observed to a greater extent for the solid wire welding fumes S1-S2 as compared with the FCW fume particles F1-F2 (Fig. 5). All of them were present only in their oxidized form in the outermost surface (5–10 nm): oxidized Fe ($2p_{3/2}$: 710.6 ± 0.8 eV; 712.9 ± 0.7 eV; 715.3 ± 0.9 eV), trivalent Cr ($2p_{3/2}$: 576.5 ± 0.6 eV; 577.5 ± 0.5 eV), hexavalent Cr ($2p_{3/2}$: 579.4 ± 0.2 eV; 580.9 eV), and oxidized Mn

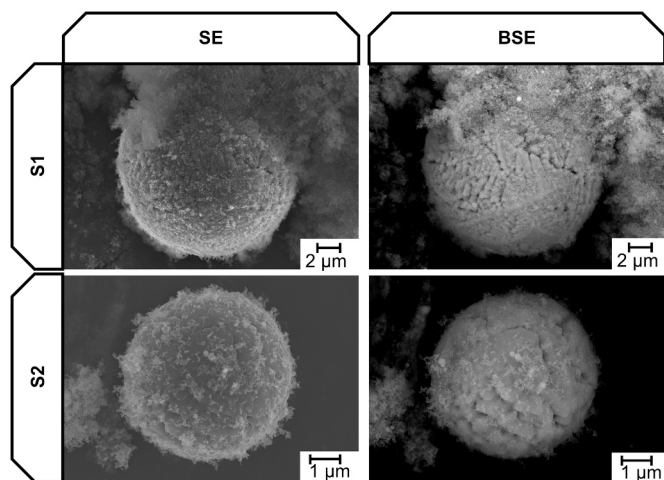


Fig. 2. SEM images showing two examples of spherical particles originating from the melt with dendrites, along with nanometer-sized particles originating from vapor. Left: SE mode, providing surface topography information; Right: BSE mode, providing average atomic contrast. Solid wire: S1, S2.

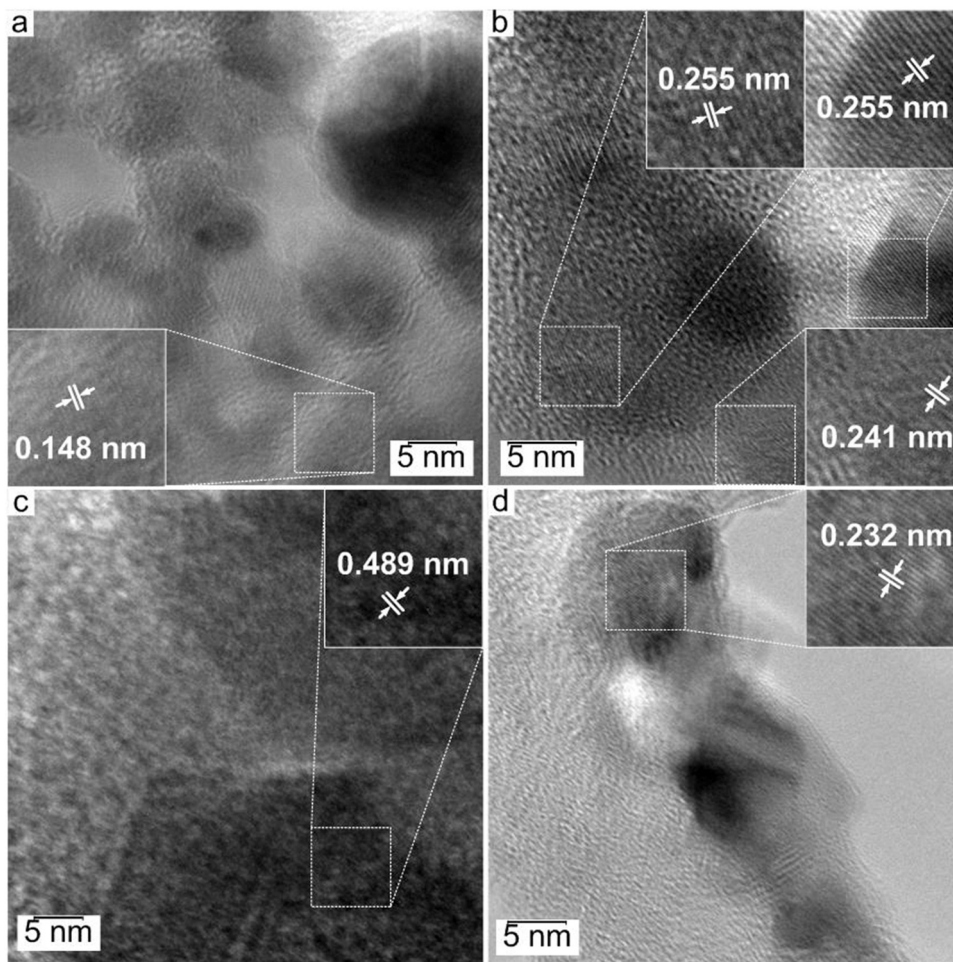


Fig. 3. High resolution TEM images showing the atomic distances in S1 (a), S2 (b), F1 (c), and F2 (d) welding fume samples.

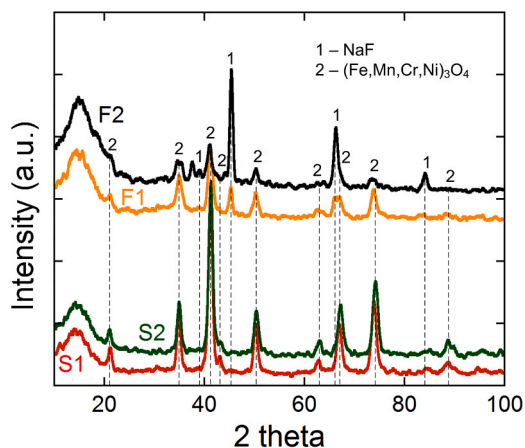


Fig. 4. XRD scan (off-set for clarity) of solid wire and the FCW fume particles (S1, S2, F1, and F2). The numbers “1” and “2” mark peaks assigned to NaF and (Fe,Mn,Cr,Ni)₃O₄ magnetite type phase, respectively.

(2p_{3/2}: 641.9 ± 0.2 eV; 645.0 ± 0.3 eV) (Biesinger et al., 2011). No Ni was observed. The peaks of trivalent and hexavalent Cr overlap partially (Biesinger et al., 2011). Fig. A5 shows an evident presence of Cr(VI), especially in the case of the welding fume particles F1-F2. The relative content of oxygen (1s: 530.3 ± 0.4 eV; 531.8 ± 0.4 eV; 533.0 ± 0.5 eV) was higher in the solid wire samples compared to the FCW samples. Relatively large surface oxide contents of Na (1s: 1068.5 ± 0.2 eV), F

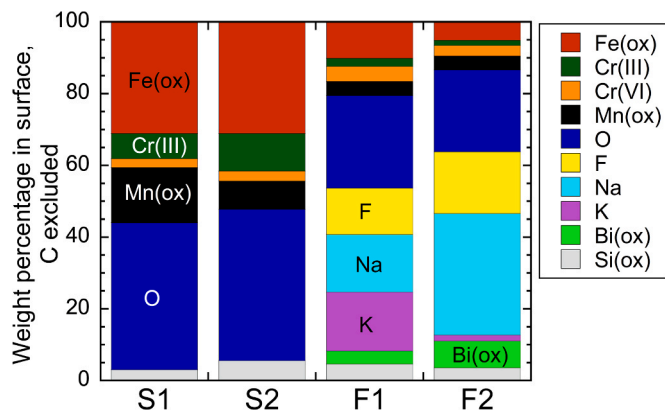


Fig. 5. Composition (outermost 5–10 nm surface) of the welding fume samples (S1, S2, F1, and F2) measured by means of XPS. Ti and Ca were additional elements of minor presence (information from the wide spectra) for the F1 and F2 samples.

(1s: 682.2 ± 0.2 eV; 684.0 eV), K (2p_{3/2}: 290.6 ± 0.7 eV; 293.3 ± 0.6 eV), and oxidized Bi (4f: 159.1 ± 0.1 eV; 164.4 ± 0.2 eV (Teterin et al., 1999)) were determined in the FCW samples F1-F2, while the same elements were absent in the solid wire samples S1 and S2. Oxidized Si (2p_{3/2}: 102.6 ± 0.5 eV) was present in all samples (Okada et al., 1998). These findings are all in agreement with previous findings of the authors (McCarrick et al., 2019; Mei et al., 2018). Sample F2

showed a higher NaF content compared to sample F1. It should be emphasized that the information depth of 5–10 nm in some cases may reflect the complete nanoparticle rather than its surface oxide only.

3.1.3. FTIR

The FTIR spectra acquired for the four different welding fume samples showed some common peaks and some peaks that were specific for certain samples. The common peaks were absorption bands centered at 470–500, 600–610, 1024, 1380, 1630, and 3440 cm^{-1} (Fig. 6). Specific peaks were observed at 375 (F2), 877–903 (F1-F2), 938 (F1-F2), 1440 (F2), and 1775 cm^{-1} (F2) (Fig. 6). The assignment of peaks for the welding fume particles is generally difficult due to the large number of possible inorganic and organic species. However, some observations can be discussed both qualitatively and semi-quantitatively.

The broad and common IR band at 3440 cm^{-1} corresponds to the stretching vibrations of adsorbed H_2O molecules, while that at 1630 cm^{-1} is most probably attributed to O-H bending vibrations (Aouissi et al., 2010). Residual water in flux-cored arc welds may originate from water and water glass in the agglomeration of the flux, but also from the cleaning of the wire surface. The bands in the region between 800 and 350 cm^{-1} can be assigned to different metal-O lattice vibrations (Cr (Zecchina et al., 1971), Mn (Kang et al., 2007; Shen and Clearfield, 1986; Feng et al., 1992), Fe (Ellid et al., 2003), and Bi (Dimitrov et al., 1994)). Due to several possibilities and a mixed oxide, it is difficult to assign them to specific metals. Some single-phase oxides can be excluded: O-Fe (from Fe_3O_4) and O-Mn groups are assigned to bands at 582 and 626 cm^{-1} , respectively (Zhou et al., 2018; Zhang et al., 2018), but they are almost absent in Fig. 6, which could reflect that they may exist as different ferrites of Mn and/or other elements. Likewise, no characteristic peaks of hematite (Fe_2O_3) (Ellid et al., 2003) or $\alpha\text{-Cr}_2\text{O}_3$ (Zecchina et al., 1971) were observed. However, when taking into account possible shifts of peak positions due to the presence of different metal oxides, the high intensity peak at 610 cm^{-1} may correspond to the most intense peak of Cr_2O_3 (NIST, 2020) or hematite.

For sample F2, the band at 375 cm^{-1} and shoulder at 450 cm^{-1} could also indicate Bi-F bonds (Kavun et al., 2000). Bi probably originates from small amounts of bismuth oxide Bi_2O_3 , added to the flux for improved slag detachability (Westin et al., 2016).

The bands at 940 and 890 cm^{-1} , only visible for F1-F2, could be assigned to Cr-O-Cr and Fe-O-H bending vibrations (Yao et al., 2003; Legrand et al., 2001), respectively. Absorption bands in the region 1100–950 cm^{-1} may be related to groups of CrO_4^{x-} ($x = 2, 3, \text{ or } 4$) (Yao et al., 2003). These bands originate from Cr-O-Cr vibrations in which the valency of the Cr ion can vary from 4 to 6 (Ratnasamy and Leonard, 1972; Fahim et al., 1981). The absorption band at 1020 cm^{-1} could indicate the organization of CrO_3 and/or Cr_2O_3 in a chromate-like structure (Fahim et al., 1981). However, more probably, this broad band (950–1250 cm^{-1}) present for all samples is mostly related to

silicon oxides and its compounds (Golden et al., 1986; Deshmukh and Aydil, 1995).

NaF is characterized by peaks at 536 cm^{-1} (Ritchie and Lew, 1964), 836, 1211, 1386 (strongest), and 1420 cm^{-1} (Gubareva, 2011). These bands were largely missing or hidden in Fig. 6. The bands at 1380 cm^{-1} (all samples, but broader for sample F1) and the strong and broad band at 1440 cm^{-1} (sample F2) could not unambiguously be assigned but is most probably related to bonds with carbon or fluorine. The strong and broad band observed at 1440 cm^{-1} for sample F2 derives most probably from carbonate (Bruckman and Wriessnig, 2013).

3.1.4. CV

In agreement with previous studies by some of the authors (Mei et al., 2018), all electroactive constituents of the surface-available phases of the welding fume particles consisted of a mixed oxide phase (Fig. 7a). Peaks that could be assigned for single-phase MnO_2 (Cha et al., 2016; Chouaib et al., 1981; Linhardt, 1998) and mono- or dichromates (Mei et al., 2018) were missing (Fig. 7a). These findings agree with the XRD measurements that did not show any evidence of either crystalline chromate species or MnO_2 . This mixed oxide phase consisted of Fe (Cha et al., 2016; Baek et al., 2001; Rico et al., 2009) and Mn (Chouaib et al., 1981; Linhardt, 1998) oxides in all cases, and in addition Bi (Pourbaix, 1984) oxides in the cases of the two FCW samples (F1 and F2) (Fig. 7b). Note that silicon (Si), titanium (Ti), and NaF species did not show any solid-solid transition peaks under the experimental conditions of the cyclic voltammetry measurements and could hence not be detected.

Missing oxidation peaks during an initial oxidation, observed for all four welding fume samples, Fig. A6, indicate that the surface oxide(s) cannot be further oxidized and are hence in their most oxidized forms. These observations are also in agreement with previous findings (Mei et al., 2018).

3.2. Total metal content and PBS-soluble metals in welding fume particles

The relative content of the main alloying elements (Fe, Cr, Ni, and Mn) of stainless steel in the welding fume was highest for the solid wire welding fume samples with 35–46 wt%, and significantly lower in the FCW welding fume samples with 14–26 wt% (Fig. 8 and Table A5). This is in agreement with previously reported studies on a larger number of welding fume samples (McCarrick et al., 2019). Despite a lower metal content in the FCW welding fume samples, the solubility of Cr(VI) expressed per mass of welding fume was significantly higher than that of the solid wire samples in PBS (Fig. 8 and Tables A6–A7). 37–58 wt% of the total Cr in the welding fume was solubilized in PBS for the FCW welding fume samples, while only 2.3–3.0 wt% of total Cr was released and stable as Cr(VI) in PBS for the solid wire welding fume samples (Table A7). These observations are in agreement with previous reports (McCarrick et al., 2019; Mei et al., 2018).

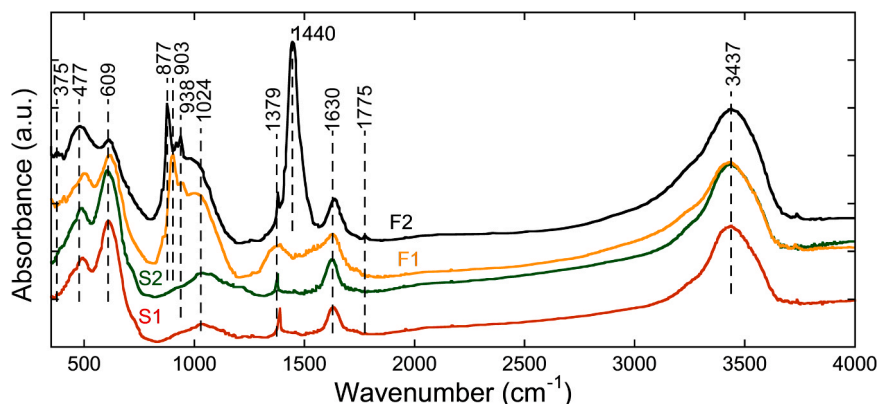


Fig. 6. FTIR spectra (off-set for clarity) for the different welding fume samples (S1, S2, F1, and F2) in the range of 350–4000 cm^{-1} .

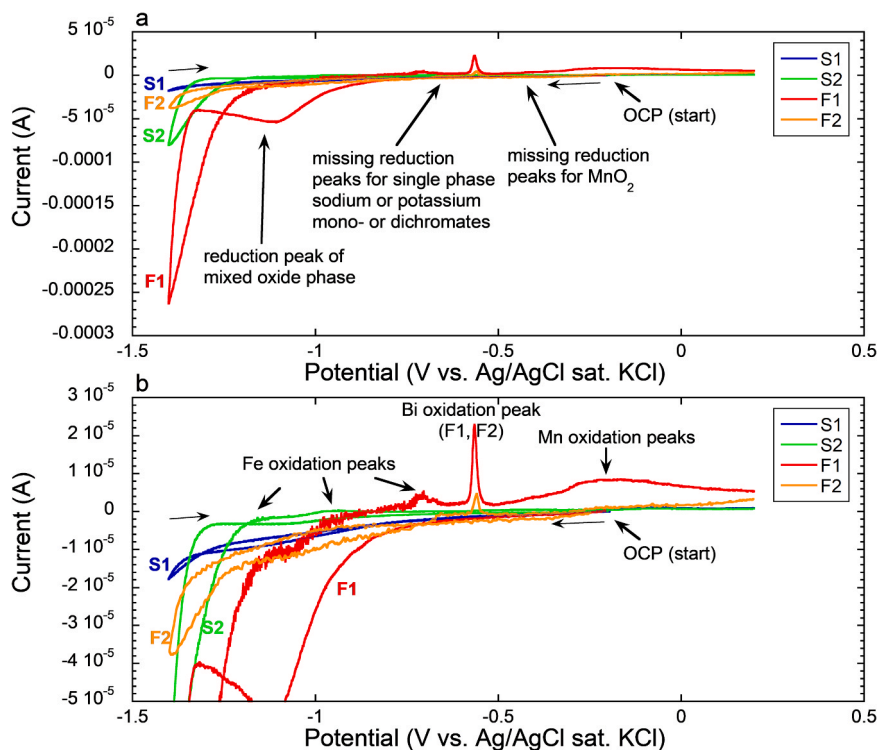


Fig. 7. Representative cyclic voltammograms (reduction from open circuit potential, OCP, followed by oxidation) at pH 13 of the welding fume particles (S1, S2, F1, and F2). Magnified voltammograms in (b) for a clearer view on the oxidation peaks. The arrows mark the start potential (OCP), which was about -0.2 V in all cases, and the reduction (a) and oxidation (b) peaks.

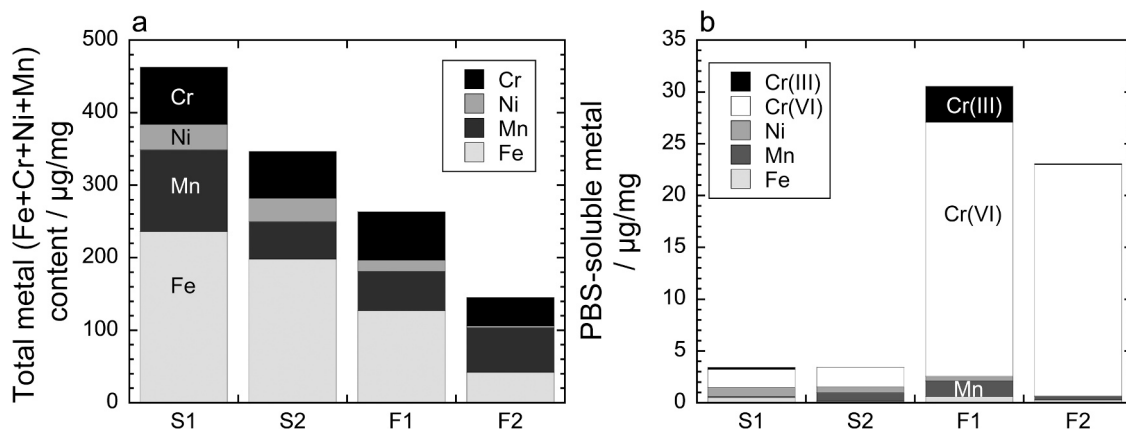


Fig. 8. Total content of Fe, Cr, Ni, and Mn in the welding fume samples (S1, S2, F1, and F2), as determined by digestion in aqua regia, (a) and the amounts of Cr(III), Cr(VI), Ni, Mn, and Fe in solution after exposure in PBS ($\text{pH } 7.3, 37^\circ\text{C}, 24\text{ h}$) (b).

It has previously been discussed whether PBS is a relevant simulant to test Cr(VI) solubility of welding fume particles (Mei et al., 2018). A bicarbonate/sodium hydroxide mixture has commonly been used as leachate medium following the ISO standards 15011 and 16740 (Cena et al., 2014, 2015; Dennis et al., 1996, 2002a, 2002b, 1997). However, that alkaline procedure has been criticized for its ability to oxidize Cr to Cr(VI) (Pedersen et al., 1987). PBS is a simulant without antioxidants that mimics the ionic strength of human blood and has a relevant physiological pH. PBS has been chosen for its unlikelihood to oxidize Cr to Cr(VI) or to reduce Cr(VI) to Cr(III) (Mei et al., 2018; Pastore et al., 2004). In order to compare different studies, the ISO 16740 procedure was followed for the four welding fume samples and compared with the PBS procedure. The trends among the different welding fumes were equal for the different procedures (Fig. 9). Consistently less Cr(VI), compared to the PBS procedure, was released during the ISO 16740

procedure, which aims at extracting all Cr(VI) (Fig. 9). This could be explained by a longer extraction time (24 h vs. 30 min) and a lower particle loading (0.1 g/L vs. 1.3 g/L) for the PBS procedure compared with the ISO 16740 procedure. However, in all, results from the two procedures were relatively comparable, which facilitates correlations and comparisons with literature findings.

3.3. Effect of fluorides on Cr(VI) and Mn release from welding fumes in PBS

Since the welding fume samples S2 and F2 showed the highest Cr(VI) release (of total Cr) in PBS within their respective groups of solid wire and FCW fumes, Table A7, these two welding fume samples were selected to investigate the effect of added fluoride ions (from NaF) on their release of Cr(VI) and Mn into PBS. These lean duplex wires also

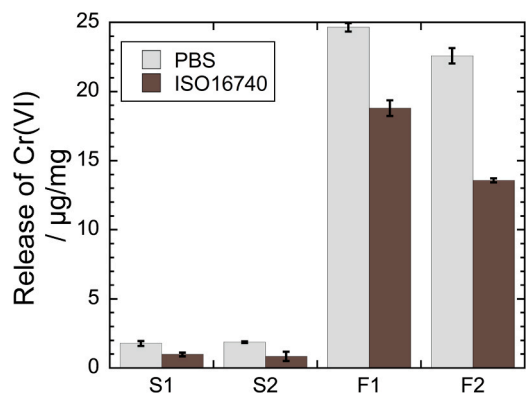


Fig. 9. Comparison of released Cr(VI) from the different welding fume samples (S1, S2, F1, and F2) during exposure in PBS for 24 h at 37 °C and during an ISO 16740 test (leaching solution at pH 12.6, 30 min, close to boiling point). The error bars show the standard deviation of independent triplicate samples.

contained about 3.5% and 5% more Cr than their respective austenitic counterpart. The release of these two species/elements was investigated, since they (i) showed the highest release in PBS and (ii) were earlier reported to link to different acute in-vitro toxic endpoints (McCarrick et al., 2019). The release of Cr(VI) of the sample F2 was not affected by varying fluoride concentration in PBS (Fig. 10). However, the soluble and released fraction of Cr(VI) of the sample S2 decreased with increasing fluoride concentration (Fig. 10). The amount of released (aqueous) Mn decreased furthermore for both particle fumes with increasing fluoride solution concentration (Fig. 10).

The two-step procedure, during which first fluorides (50 mg F/L) were adsorbed on the sample S1 followed by re-dispersion in PBS, resulted in non-detectable Cr(VI) levels (data not shown).

Table 3 presents predictions of the chemical speciation of Cr, Mn, Fe, and Ni in PBS at different redox potentials (simulating any co-released species of oxidative nature) as determined by chemical speciation modeling (JESS). Mn and Fe were not predicted to be stable in solution at any conditions, while Ni was predicted soluble and Cr soluble as Cr(VI) at higher redox potential. A higher redox potential can be achieved by dissolved oxygen or co-released oxidative species, such as permanganate.

The effect of the presence of fluorides on the chemical speciation of Cr and Mn was also investigated by chemical speciation modeling. Data was available for solid Cr and Mn-fluoride compounds in the database. No effect was observed. The predicted chemical speciation of Cr and Mn in the presence of 1–50 mg F/L in PBS was equal to corresponding predictions in PBS.

Fluoride-metal complexes could have been formed and resulted in

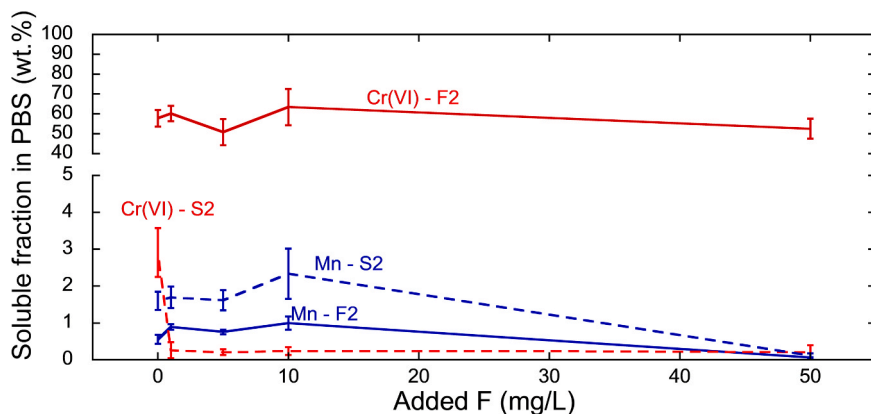


Fig. 10. Soluble Cr(VI) or Mn of total Cr or Mn (determined after digestion) in PBS with 0, 1, 5, 10, and 50 mg/L added F (from NaF) for the welding fume samples S2 and F2. The error bars show the standard deviation of triplicate samples.

Table 3

Results of chemical speciation modeling at two different redox potential representing a normal redox potential in water (pe 5) and oxidative conditions (pe 10) in PBS (pH 7.3) at 25 °C and atmospheric pressure. Aqueous species are marked in bold. s – solid; SHE – standard hydrogen electrode.

Metal	pe 5 (296 mV vs. SHE)	pe 10 (592 mV vs. SHE)
Cr	100% (19.2 µM) CrOOH (s)	69% (13.3 µM) CrO₄²⁻ , 26% NaCrO₄ , 3% HCrO₄⁻ , 2% KCrO₄
Mn	100% (9.10 µM) MnHPO ₄ (s)	
Fe	100% (17.9 µM) Fe ₄ (OH) ₃ (PO ₄) ₃ ·12H ₂ O (s)	
Ni	48% (1.64 µM) Ni²⁺ , 42% NiHPO₄ , 8% NiCl⁺ , 2% NiCl₂	

precipitation at higher fluoride concentrations. It is in this context important to note that 50 mg F/L corresponds to similar or a higher loading of the sum of Mn, Cr, Ni, and Fe mass in the given experimental conditions (0.1 g/L welding fume with 15–35 wt% metal content) – hence, an excess of fluorides. If metal-fluoride complexes would form, precipitation could be expected. Alternatively, a protective surface layer of metal-fluoride complexes could be expected to hinder further dissolution of Mn and Cr(VI) from the welding fume particles. Such a case would be supported by the experimental observation of a reduced Cr(VI) and Mn solubility in some cases with increasing fluoride content in PBS (Fig. 10), and speciation database and literature observations of the formation of stable metal-fluorides (Fackler and Chawla, 1964; Parkinson and Williams, 1950; Wanklyn, 1969; Azad and Sreedharan, 1987). However, these complexes are according to the speciation prediction not the predominant species formed in PBS and under the experimental conditions. An alternative interpretation would be that the fluoride ions change the solution redox potential. This would not be possible directly (fluorides are not electroactive under the experimental conditions), but indirectly, e.g. by influencing the access to trivalent iron. Fluorides, especially in the presence of chlorides, can damage metal oxides and increase the dissolution of iron oxides (Mirjalili et al., 2013; Li et al., 2007; Pahlavan et al., 2016), which can have a reductive effect (Shetlemore and Bundy, 2001) and hence reduce the release of chromates and permanganates.

3.4. In-vitro cytotoxicity and genotoxicity

In agreement with previous observations (McCarrick et al., 2019), the FCW samples F1 and F2, which released the highest amounts and percentages of Cr(VI), were significantly more cytotoxic and genotoxic as compared to controls and to the solid wire samples S1-S2 (Fig. 11). Cytotoxic effects were significantly increased compared with the control for both FCW samples (F1-F2) at 25 µg/mL and above in a dose-response manner. Close to 100% cytotoxicity was observed in the human bronchial epithelial cells at 100 µg/mL of the F1 and F2 particles after 24 h

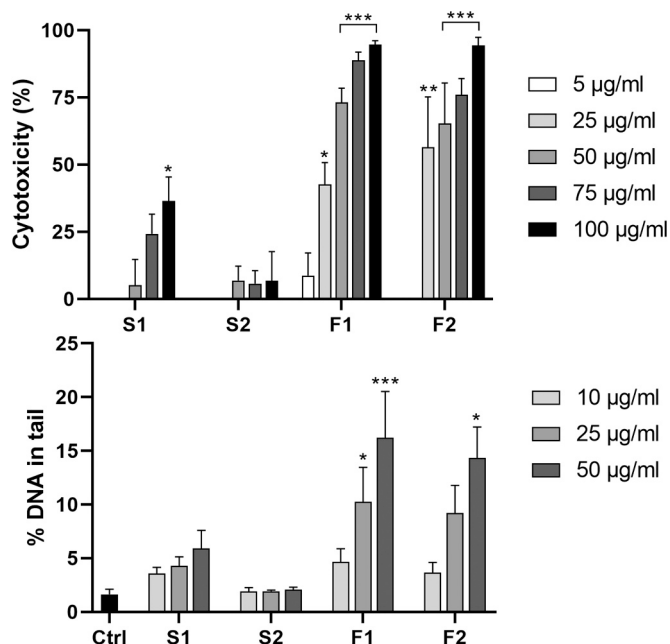


Fig. 11. Cytotoxicity at 24 h (top) and genotoxicity at 3 h (bottom) in human bronchial epithelial cells as estimated based on the Alamar blue assay and the comet assay, respectively, for different doses and the four different welding fume samples. Triton X (1%) and NiO (25 µg/mL) were used as positive controls for cyto- and genotoxicity, respectively, and resulted in significant increase ($P < 0.001$). The results are presented as mean \pm SD of three or four independent experiments ($n = 3-4$). Ctrl - negative control; * $P < 0.05$; ** $P < 0.01$; *** $P < 0.001$.

incubation. In contrast, no cytotoxic effect was observed for the sample S2, and significant increased cytotoxic effects were observed only for the highest exposure of 100 µg/mL for the sample S1 (Fig. 11). A dose-response increase in DNA damage was observed for the FCW samples F1 and F2 at 3 h exposure, where significant genotoxic effects were observed starting at a dose of 25 µg/mL and 50 µg/mL for the F1 and F2 samples, respectively (Fig. 11). No genotoxic effects were observed following exposure to solid wire S1-S2 samples.

No cytotoxic effect was observed for the control experiment with up to 20 µg F/mL (from NaF) (data not shown).

3.5. Further discussion

The low release of Ni from welding fume particles into PBS observed experimentally can primarily be explained by its absence in the surface oxide (c.f. Section 3.1). A previous study reported an increased release of Ni for the smallest size fraction of the welding fume particles (Mei et al., 2018) due to a generally higher solubility of smaller particles that have a strongly increased surface-to-bulk ratio (Misra et al., 2012; Kuech et al., 2016). In agreement with expectations, Fe was not soluble under the given experimental conditions (Table 3, Fig. 8). Mn was not expected to be soluble either but was to some extent released and detected, possibly due to slow kinetics of precipitation. Cr was only at high oxidative potentials [as Cr(VI)] expected to be in an aqueous (non-solid) form (Table 3). Cyclic voltammetry revealed fully oxidized metal oxides on all welding fume particles. XPS revealed the presence of highly (IV/VI/-VII-valent) oxidized Mn species that could potentially provide a strong oxidative effect and induce the chemical environment necessary to release Cr(VI). The presence of several Mn species, including highly valent species, is in agreement with previous characterization findings of welding fume (Hanley et al., 2017; Andrews et al., 2015). The ability of Mn-containing oxides to oxidize Cr to Cr(VI) and keep it oxidized is a known geochemical phenomenon of Cr-containing minerals, soils, and

their release of Cr(VI) to e.g. groundwater (Hausladen and Fendorf, 2017; Oze et al., 2007; Weaver et al., 2002; Wu et al., 2007).

This study stresses that studies of welding fumes should not only focus on separate effects but rather on synergistic effects of environmental conditions that influence the solubility of highly valent Mn and Cr(VI) species. Highly valent Mn oxides, especially soluble oxides, could potentially support the dissolution of Cr species as Cr(VI) under physiologically relevant conditions.

A clear correlation has previously been observed between the presence of NaF and/or K-containing fluorides in the flux and the release of Cr(VI) (c.f. Section 1). The welding fume sample F2, which contained significantly more NaF as compared to the other FCW sample F1, did not release higher amounts of Cr(VI) when normalized per welding fume mass, but did release higher amounts of Cr(VI) in PBS when normalized to the total Cr content. Both FCW samples released significantly more Cr(VI) into PBS when compared to their solid wire reference samples. This study suggests that this is not directly caused by the NaF or fluoride content in FCW fumes. In this study, Na did not contribute to the formation of crystalline and easily soluble chromates, such as $\text{Na}_2\text{Cr}_2\text{O}_7$. The absence of these phases was confirmed by XRD and CV and the results are in agreement with previous observations for similar welding fumes (Mei et al., 2018), but in contrast to studies on other or similar welding fumes (Floros, 2018; Minni et al., 1984; Sowards, 2006). Instead, Cr(VI) was incorporated in a mixed oxide phase (a spinel), most probably amorphous, since Cr(VI) cannot be incorporated in a crystalline magnetite-type structure (Floros, 2018). Solution-added fluorides did not increase the release and solution-detected amounts of Cr(VI), but resulted instead in a reduced amount of Cr(VI) in solution for one of the two tested fume particle samples. These fluorides furthermore resulted in a reduced Mn release for both investigated fume samples. Considering the chemical speciation modeling results, this is most probably related to an influence of the fluorides on the redox potential, for instance via increased surface access and solubility of iron oxides. NaF was not cytotoxic itself. This study suggests hence that NaF or other easily soluble fluorides do not directly increase the Cr(VI) solubility of welding fume particles in PBS.

There is clear evidence that the solubility, especially of Cr(VI) and Mn, of welding fume particles in PBS and similar media is linked to acute in-vitro cytotoxic and genotoxic outcomes (McCarrick et al., 2019; Olgun et al., 2020). This study confirmed those observations. However, it should be emphasized that long-term effects, such as lung cancer, have been primarily observed for non-soluble species such as iron oxides (Falcone et al., 2018; Moulin et al., 1993). In addition, the small size of the welding fume particles, alone, is causing increased cell uptake and possible short and long-term adverse health effects (Block and Calderón-Garcidueñas, 2009; VanWinkle et al., 2009; Shi et al., 2012; Carlander et al., 2019). Still, there is an advantage to reduce the acute hazard of welding fume already at the source. The welding process and electrode composition appear to be the most important factors influencing the solubility of Mn and Cr(VI). This is in agreement with previous studies that also highlight the effect of the weldability, fume formation rate, and arc stability, which in turn are influenced by the shielding gas and filler metal formulation (Floros, 2016; Vishnu et al., 2018; Keane et al., 2016; Pires et al., 2007). As the composition of the four electrodes used in this study was considerably different, it was not possible to draw any conclusions regarding the slag concepts. This aspect would be very interesting to evaluate in future studies.

4. Conclusions

This study aimed at exploring the role of NaF (or other fluorides) in flux-cored wire electrodes, as compared to solid wire electrodes, on the stainless steel welding fume composition, the solubility of Cr, Cr(VI), Mn, Ni, and Fe released from welding fume particles into PBS, cytotoxicity, and genotoxicity. The following main conclusions can be drawn:

The welding fume particles generated from wire electrodes containing NaF (and other fluorides) released significantly higher amounts of Cr(VI) into both PBS and an alkaline medium (ISO 16740). This was associated with increased cytotoxicity and genotoxicity in-vitro. These responses were not necessarily a direct cause of Na/K or F ions. Crystalline Na or K-containing chromates were not observed in this study. Cr(VI) was most probably incorporated in an amorphous mixed oxide (spinel). Fluorides did not increase the solubility of Cr(VI) in welding fume particles but were able to reduce the release of Mn for both solid wire and FCW fume particles and to reduce the release of Cr(VI) from solid wire fume particles into PBS. Chemical speciation modeling suggested that metal fluoride complexes were not formed. Instead, an indirect effect, such as higher surface access and solubility of iron oxides caused by fluorides, could be a contributing factor to a reduced solubility of Mn and Cr(VI) in the presence of excess NaF. This study suggests that highly valent soluble Mn species, such as permanganates, contribute to the solubility of Cr(VI) in welding fume particles under physiological relevant conditions.

Funding

This work was supported by the foundation ÅForsk [grant numbers 17-387; 19-323], Sweden's innovation agency VINNOVA [grant numbers 2017-02519; 2018-02383], the Swedish Foundation for Strategic Research [grant number FFL18-0173], the Swedish Steel Association Jernkontoret [grant number Prytziska fonden 2-2019], the Ministry of Science and Higher Education of the Russian Federation in the framework of Increase Competitiveness Program of NUST "MISIS" [grant number K2-2019-007], and the Swedish Research Council [grant numbers 2014-4598; 2017-03931].

CRediT authorship contribution statement

Y.S. Hedberg: Conceptualization, Formal analysis, Investigation, Methodology, Project administration, Resources, Supervision, Validation, Visualization, Writing - original draft, Writing - review & editing, Funding acquisition. **Z. Wei:** Investigation, Methodology, Validation, Writing - review & editing. **S. McCarrick:** Investigation, Formal analysis, Methodology, Validation, Visualization, Writing - original draft. **V. Romanovski:** Investigation, Methodology, Resources, Visualization, Writing - original draft. **J. Theodore:** Investigation. **E. Westin:** Resources, Writing - review & editing. **R. Wagner:** Resources, Writing - review & editing. **K.-A. Persson:** Conceptualization, Writing - review & editing, Funding acquisition. **H.L. Karlsson:** Conceptualization, Methodology, Supervision, Writing - review & editing, Funding acquisition. **I. Odnevall Wallinder:** Investigation, Formal analysis, Writing - review & editing.

Declaration of Competing Interest

The authors declare that they have no known competing financial interests or personal relationships that could have appeared to influence the work reported in this paper.

Acknowledgements

Naza Alexis, Anna Lund, Raghda Kalifa, all KTH students, are highly acknowledged for pilot studies of fluoride additions as part of their bachelor thesis. Mathias Lundin, Swedish Welding Commission, is highly acknowledged for valuable discussions. Ivan Barker, Surface Science Western, is highly acknowledged for the high-resolution SEM analysis.

Appendix A. Supporting information

Supplementary data associated with this article can be found in the

online version at doi:10.1016/j.jhazmat.2021.125273.

References

- Alexander, L., Klug, H.P., 1950. Determination of crystallite size with the X-Ray spectrometer. *J. Appl. Phys.* 21, 137–142.
- Andersson, M., Slunga Järholm, L., Järholm, B., 2019. Kunskaps sammanställning 2019:3: Arbetsrelaterad dödlighet – delrapport 1. Beräkning av antalet dödsfall 2016 uppdelat på olika exponeringar i arbetet, Swedish Work Environment Authority, (<https://www.av.se/globalassets/filer/publikationer/kunskaps-sammanstallningar/arbetsrelaterad-dodlighet-rap-2019-4-del-2.pdf>).
- Andrews, R.N., Keane, M., Hanley, K.W., Feng, H.A., Ashley, K., 2015. Manganese speciation of laboratory-generated welding fumes. *Anal. Methods* 7, 6403–6410.
- Antonini, J.M., Lawryk, N.J., Murthy, G.G.K., Brain, J.D., 1999. Effect of welding fume solubility on lung macrophage viability and function in vitro. *J. Toxicol. Environ. Health A* 58, 343–363.
- Antonini, J.M., Lewis, A.B., Roberts, J.R., Whaley, D.A., 2003. Pulmonary effects of welding fumes: review of worker and experimental animal studies. *Am. J. Ind. Med.* 43, 350–360.
- Antonini, J.M., Taylor, M.D., Zimmer, A.T., Roberts, J.R., 2004. Pulmonary responses to welding fumes: role of metal constituents. *J. Toxicol. Environ. Health A* 67, 233–249.
- Antonini, J.M., Leonard, S.S., Roberts, J.R., Solano-Lopez, C., Young, S.-H., Shi, X., Taylor, M.D., 2005. Effect of stainless steel manual metal arc welding fume on free radical production, DNA damage, and apoptosis induction. *Mol. Cell. Biochem.* 279, 17–23.
- Aouissi, A., Al-Othman, Z.A., Bayahia, H., 2010. Ethyl benzene dehydrogenation in the presence of carbon dioxide over Fe₂O₃-Cr₂O₃ catalyst. *Asian J. Chem.* 22, 4873.
- Azad, A., Sreedharan, O., 1987. Comparative emf study of CaF₂ and β-alumina cells with Ni/NiF₂ and Fe/FeF₂ or Cr/CrF₂ electrodes. *J. Appl. Electrochem.* 17, 949–955.
- Baek, W.-C., Kang, T., Sohn, H.-J., Kho, Y.T., 2001. In situ surface enhanced Raman spectroscopic study on the effect of dissolved oxygen on the corrosion film on low carbon steel in 0.01 M NaCl solution. *Electrochim. Acta* 46, 2321–2325.
- Biesinger, M.C., Payne, B.P., Grosvenor, A.P., Lau, L.W.M., Gerson, A.R., Smart, R.S.C., 2011. Resolving surface chemical states in XPS analysis of first row transition metals, oxides and hydroxides: Cr, Mn, Fe, Co and Ni. *Appl. Surf. Sci.* 257, 2177–21730.
- Block, M.L., Calderón-Garcidueñas, L., 2009. Air pollution: mechanisms of neuroinflammation and CNS disease. *Trends Neurosci.* 32, 506–516.
- Bruckman, V.J., Wriessnig, K., 2013. Improved soil carbonate determination by FT-IR and X-ray analysis. *Environ. Chem. Lett.* 11, 65–70.
- Carlander, U., Midander, K., Hedberg, Y.S., Johanson, G., Bottai, M., Karlsson, H.L., 2019. Macrophage-assisted dissolution of gold nanoparticles. *ACS Appl. Bio Mater.* 2, 1006–1016.
- Cena, L.G., Chisholm, W.P., Keane, M.J., Cumpston, A., Chen, B.T., 2014. Size distribution and estimated respiratory deposition of total chromium, hexavalent chromium, manganese, and nickel in gas metal arc welding fume aerosols. *Aerosol Sci. Technol.* 48, 1254–1263.
- Cena, L.G., Chisholm, W.P., Keane, M.J., Chen, B.T., 2015. A field study on the respiratory deposition of the nano-sized fraction of mild and stainless steel welding fume metals. *J. Occup. Environ. Hyg.* 12, 721–728.
- Cha, Y., Hedberg, Y., Mei, N., Olofsson, U., 2016. Airborne wear particles generated from conductor rail and collector shoe contact: influence of sliding velocity and particle size. *Tribol. Lett.* 64, 40.
- Chouaib, F., Cauquil, O., Lamache, M., 1981. Comportement électrochimique d'oxydes de manganèse, en milieu alcalin. *Electrochim. Acta* 26, 325–328.
- Coggon, D., Palmer, K.T., 2016. Are welders more at risk of respiratory infections? *Thorax* 71, 581–582.
- Dennis, J., French, M., Hewitt, P., Mortazavi, S., Redding, A., 1996. Reduction of hexavalent chromium concentration in fumes from metal cored arc welding by addition of reactive metals. *Ann. Occup. Hyg.* 40, 339–344.
- Dennis, J.H., Mortazavi, S.B., French, M.J., Hewitt, P.J., Redding, C.R., 1997. The effects of welding parameters on ultraviolet light emissions, ozone and CrVI formation in MIG welding. *Ann. Occup. Hyg.* 41, 95–104.
- Dennis, J.H., French, M.J., Hewitt, P.J., Mortazavi, S.B., Redding, C.A., 2002. Control of exposure to hexavalent chromium and ozone in gas metal arc welding of stainless steels by use of a secondary shield gas. *Ann. Occup. Hyg.* 46, 43–48.
- Dennis, J.H., French, M.J., Hewitt, P.J., Mortazavi, S.B., Redding, C.A., 2002. Control of occupational exposure to hexavalent chromium and ozone in tubular wire arc-welding processes by replacement of potassium by lithium or by addition of zinc. *Ann. Occup. Hyg.* 46, 33–42.
- Deshmukh, S.C., Aydil, E.S., 1995. Investigation of SiO₂ plasma enhanced chemical vapor deposition through tetraethoxysilane using attenuated total reflection Fourier transform infrared spectroscopy. *J. Vac. Sci. Technol. A* 13, 2355–2367.
- Di Bucchianico, S., Cappellini, F., Le Bihanic, F., Zhang, Y., Dreij, K., Karlsson, H.L., 2017. Genotoxicity of TiO₂ nanoparticles assessed by mini-gel comet assay and micronucleus scoring with flow cytometry. *Mutagenesis* 32, 127–137.
- Dimitrov, V., Dimitriev, Y., Montenero, A., 1994. IR spectra and structure of V₂O₅-GeO₂-Bi₂O₃ glasses. *J. Non-Cryst. Solids* 180, 51–57.
- Ellid, M., Murayed, Y., Zoto, M., Musić, S., Popović, S., 2003. Chemical reduction of hematite with starch. *J. Radioanal. Nucl. Chem.* 258, 299–305.
- Ellingsen, D.G., Chashchin, M., Seljeflot, I., Berlinger, B., Chashchin, V., Stockfelt, L., Thomassen, Y., 2019. A study of atherothrombotic biomarkers in welders. *Int. Arch. Occup. Environ. Health* 92, 1023–1031.
- Fackler Jr., J., Chawla, I., 1964. Spectra of manganese (III) complexes. I. Aquomanganese (III) ion and hydroxide, fluoride, and chloride complexes. *Inorg. Chem.* 3, 1130–1134.

- Fahim, R., Gabr, R., Zaki, M., Mansour, S., 1981. Nonstoichiometry and surface characterization of chromia gel. *J. Colloid Interfaces Sci.* 81, 468–476.
- Falcone, L.M., Erdely, A., Salmen, R., Keane, M., Battelli, L., Kodali, V., Bowers, L., Stefaniak, A.B., Kashon, M.L., Antonini, J.M., 2018. Pulmonary toxicity and lung tumorigenic potential of surrogate metal oxides in gas metal arc welding–stainless steel fume: iron as a primary mediator versus chromium and nickel. *PLoS One* 13, e0209413.
- Feng, Q., Miyai, Y., Kanoh, H., Ooi, K., 1992. Lithium (1+) extraction/insertion with spinel-type lithium manganese oxides. Characterization of redox-type and ion-exchange-type sites. *Langmuir* 8, 1861–1867.
- Floros, N., 2018. Welding fume main compounds and structure. *Weld. World* 62, 311–316.
- Floros, N., 2016. Hexavalent chromium in stainless steel solid wire welding fumes, in: Commission VIII - Health, Safety, and Environment, International Institute of Welding.
- Gliga, A.R., Skoglund, S., Odnevall Wallinder, I., Fadeel, B., Karlsson, H.L., 2014. Size-dependent cytotoxicity of silver nanoparticles in human lung cells: the role of cellular uptake, agglomeration and Ag release. *Part. Fibre Toxicol.* 11, 11.
- Golden, D., Chen, C., Dixon, J., 1986. Synthesis of todorokite. *Science* 231, 717–719.
- Gomes, J.F., Albuquerque, P.C., Miranda, R.M., Santos, T.G., Vieira, M.T., 2012. Comparison of deposited surface area of airborne ultrafine particles generated from two welding processes. *Inhal. Toxicol.* 24, 774–781.
- Gomes, J.F.P., Albuquerque, P.C.S., Miranda, R.M.M., Vieira, M.T.F., 2012. Determination of airborne nanoparticles from welding operations. *J. Toxicol. Environ. Health A* 75, 747–755.
- Gubareva, T.B., 2011. Спектры поглощения щелочно-галогенных кристаллов после радиолитиза системы “кристалл-воздух” [Absorption spectra of alkali-halide crystals after radiolysis of the “crystal-air” system]. Системы. Методы. Технологии 124–131 (https://brstu.ru/static/unit/journal_smt/docs/number111/124-131.pdf).
- Guo, N., Xu, C., Du, Y., Chen, H., Fu, Y., Feng, J., 2019. Influence of calcium fluoride on underwater wet welding process stability. *Weld. World* 63, 107–116.
- Hanley, K.W., Andrews, R., Bertke, S., Ashley, K., 2017. Exploring manganese fractionation using a sequential extraction method to evaluate welders’ gas metal arc welding exposures during heavy equipment manufacturing. *Ann. Work Expo. Health* 61, 123–134.
- Hausladen, D.M., Fendorf, S., 2017. Hexavalent chromium generation within naturally structured soils and sediments. *Environ. Sci. Technol.* 51, 2058–2067.
- Hedmer, M., Karlsson, J.-E., Andersson, U., Jacobsson, H., Nielsen, J., Tinnerberg, H., 2014. Exposure to respirable dust and manganese and prevalence of airways symptoms, among Swedish mild steel welders in the manufacturing industry. *Int. Arch. Occup. Environ. Health* 87, 623–634.
- Honaryar, M.K., Lunn, R.M., Luce, D., Ahrens, W., Hansen, J., Bouaoun, L., Loomis, D., Byrnes, G., Vilahur, N., Stayner, L., 2019. Welding fumes and lung cancer: a meta-analysis of case-control and cohort studies. *Occup. Environ. Med.* 76, 422–431.
- IARC, 2018. Welding, molybdenum trioxide, and indium tin oxide, International Agency for Research on Cancer (IARC), World Health Organization.
- Ibelft, E., Bonde, J.P., Hansen, J., 2010. Exposure to metal welding fume particles and risk for cardiovascular disease in Denmark: a prospective cohort study. *Occup. Environ. Med.* 67, 772–777.
- ISO, 2017b. ISO 17075-1, Leather - chemical determination of chromium(VI) content in leather - part 1: colorimetric method.
- ISO, 2017a. Health and safety in welding and allied processes - laboratory method for sampling fume and gases, ISO 15011.
- ISO, 2005. Workplace air - determination of hexavalent chromium in airborne particulate matter - method by ion chromatography and spectrophotometric measurement using diphenyl carbazide, ISO 16740.
- Jeong, J.Y., Park, J.S., Kim, P.G., 2016. Characterization of total and size-fractionated manganese exposure by work area in a shipbuilding yard. *Saf. Health Work* 7, 150–155.
- Kang, L., Zhang, M., Liu, Z.-H., Ooi, K., 2007. IR spectra of manganese oxides with either layered or tunnel structures. *Spectrochim. Acta A* 67, 864–869.
- Kavun, V.Y., Merkulov, E., Goncharuk, V., Ignat’eva, L., 2000. Synthesis, structure and fluorine ions dynamics in glasses on the base of indium and bismuth trifluorides. *Fiz. Khimiya Stekla* 26, 414–419.
- Keane, M., Siert, A., Stone, S., Chen, B.T., 2016. Profiling stainless steel welding processes to reduce fume emissions, hexavalent chromium emissions and operating costs in the workplace. *J. Occup. Environ. Hyg.* 13, 1–8.
- Kendzia, B., Pesch, B., Pohlbeln, H., Ahrens, W., Wichmann, H., Taeger, D., Zschiesche, W., Behrens, T., Jöckel, K.H., Brüning, T., 2020. Kumulative Gefahrstoffexpositionen beim Schweißen und dessen Auswirkungen auf das Lungenkrebisrisiko. *Pneumologie* 74, FV219.
- Knobloch, J., Casjens, S., Lehnert, M., Yanik, S.D., Körber, S., Lotz, A., Rupp, J., Raulf, M., Zschiesche, W., Weiss, T., 2020. Exposure to welding fumes suppresses the activity of T-helper cells. *Environ. Res.* 189, 109913.
- Kuech, T.R., Hamers, R.J., Pedersen, J.A., 2016. Chemical transformation of metal, metal oxide, and metal chalcogenide nanoparticles in the environment. In: Xing, B., Vecitis, C.D., Senesi, N. (Eds.), *Engineered Nanoparticles and the Environment: Biophysical-Chemical Processes and Toxicity*. John Wiley & Sons Inc, pp. 261–291.
- Legrand, L., Sagon, G., Lecomte, S., Chausse, A., Messina, R., 2001. A Raman and infrared study of a new carbonate green rust obtained by electrochemical way. *Corros. Sci.* 43, 1739–1749.
- Leonard, S.S., Chen, B.T., Stone, S.G., Schwegler-Berry, D., Kenyon, A.J., Frazer, D., Antonini, J.M., 2010. Comparison of stainless and mild steel welding fumes in generation of reactive oxygen species. *Part. Fibre Toxicol.* 7, 32.
- Li, X., Wang, J., Han, E.-h., Ke, W., 2007. Influence of fluoride and chloride on corrosion behavior of NiTi orthodontic wires. *Acta Biomater.* 3, 807–815.
- Linhardt, P., 1998. Electrochemical identification of higher oxides of manganese in corrosion relevant deposits formed by microorganisms. *Mater. Sci. Forum* 289, 1267–1274.
- May, P.M., 2015. JESS at thirty: strengths, weaknesses and future needs in the modelling of chemical speciation. *Appl. Geochem.* 55, 3–16.
- McCarrick, S., Wei, Z., Moelijker, N., Derr, R., Persson, K.-A., Hendriks, G., Odnevall Wallinder, I., Hedberg, Y.S., Karlsson, H.L., 2019. High variability in toxicity of welding fume nanoparticles from stainless steel in lung cells and reporter cell lines: the role of particle reactivity and solubility. *Nanotoxicology* 13, 1293–1309.
- Mei, N., Belleville, L., Cha, Y., Olofsson, U., Odnevall Wallinder, I., Persson, K.-A., Hedberg, Y., 2018. Size-separated particle fractions of stainless steel welding fume particles – a multi-analytical characterization focusing on surface oxide speciation and release of hexavalent chromium. *J. Hazard. Mater.* 342, 527–535.
- Minni, E., Gustafsson, T.E., Koponen, M., Kalliomaki, P.-L., 1984. A study of the chemical structure of particles in the welding fumes of mild and stainless steel. *J. Aerosol Sci.* 15, 57–68.
- Mirjalili, M., Momeni, M., Ebrahimi, N., Moayed, M.H., 2013. Comparative study on corrosion behaviour of nitinol and stainless steel orthodontic wires in simulated saliva solution in presence of fluoride ions. *Mater. Sci. Eng. C* 33, 2084–2093.
- Misra, S.K., Dybowska, A., Berhanu, D., Luoma, S.N., Valsami-Jones, E., 2012. The complexity of nanoparticle dissolution and its importance in nanotoxicological studies. *Sci. Total Environ.* 438, 225–232.
- Mocevic, E., Kristiansen, P., Bonde, J.P., 2015. Risk of ischemic heart disease following occupational exposure to welding fumes: a systematic review with meta-analysis. *Int. Arch. Occup. Environ. Health* 88, 259–272.
- Moroni, B., Viti, C., 2009. Grain size, chemistry, and structure of fine and ultrafine particles in stainless steel welding fumes. *J. Aerosol Sci.* 40, 938–949.
- Moulin, J.J., Wild, P., Mantout, B., Fournier-Betz, M., Mur, J.M., Smagge, G., 1993. Mortality from lung cancer and cardiovascular diseases among stainless-steel producing workers. *Cancer Cause Control* 4, 75–81.
- NIST, NIST Chemistry WebBook, SRD 69, Chromium oxide. (<https://webbook.nist.gov/cgi/cbook.cgi?ID=C1308389&Mask=80>). (Accessed 22 December 2020).
- Okada, K., Kameshima, Y., Yasumori, A., 1998. Chemical shifts of silicon X-ray photoelectron spectra by polymerization structures of silicates. *J. Am. Ceram. Soc.* 81, 1970–1972.
- Olgun, N.S., Morris, A.M., Bowers, L.N., Stefaniak, A.B., Friend, S.A., Reznik, S.E., Leonard, S.S., 2020. Mild steel and stainless steel welding fumes elicit pro-inflammatory and pro-oxidant effects in first trimester trophoblast cells. *Am. J. Reprod. Immunol.* 83, e13221.
- Oze, C., Bird, D.K., Fendorf, S., 2007. Genesis of hexavalent chromium from natural sources in soil and groundwater. *Proc. Natl. Acad. Sci. USA* 104, 6544.
- Pahlavan, S., Moazen, S., Taji, I., Saffar, K., Hamrah, M., Moayed, M.H., Mollazadeh Beidokhti, S., 2016. Pitting corrosion of martensitic stainless steel in halide bearing solutions. *Corros. Sci.* 112, 233–240.
- Parkinson Jr., W., Williams, F.E., 1950. The absorption spectra of manganese fluoride, zinc fluoride, and manganese-activated zinc fluoride. *J. Chem. Phys.* 18, 534–537.
- Pastore, P., Favaro, G., Ballardini, A., Danieleto, D., 2004. Evidence of Cr(VI) formation during analysis of leather: proposal of an alternative method of analysis through the ion-chromatographic approach and post-column reaction. *Talanta* 63, 941–947.
- Pedersen, B., Thomsen, E., Stern, R., 1987. Some problems in sampling, analysis and evaluation of welding fumes containing Cr (VI). *Ann. Occup. Hyg.* 31, 325–338.
- Pires, I., Quintino, L., Miranda, R., 2007. Analysis of the influence of shielding gas mixtures on the gas metal arc welding metal transfer modes and fume formation rate. *Mater. Des.* 28, 1623–1631.
- Pourbaix, M., 1984. Electrochemical corrosion of metallic biomaterials. *Biomaterials* 5, 122–134.
- Praveen, P., Yarlagadda, P.K.D.V., Kang, M.J., 2005. Advancements in pulse gas metal arc welding. *J. Mater. Process. Technol.* 164–165, 1113–1119.
- Ratnasamy, P., Leonard, A., 1972. Structural evolution of chromia. *J. Phys. Chem.* 76, 1838–1843.
- Rico, Y., Bidegain, J.C., Elsner, C., 2009. Synthetic and natural Iron oxide characterization through microparticle voltammetry. *Geofis. Int.* 48, 221–235.
- Ritchie, R., Lew, H., 1964. Infrared spectra of NaF and KF. *Can. J. Phys.* 42, 43–52.
- Rushton, L., Bagga, S., Bevan, R., Brown, T., Cherrie, J., Holmes, P., Fortunato, L., Hutchings, S., Slack, R., Van Tongeren, M., Young, C., Evans, G.S., 2012. The burden of occupational cancer in Great Britain, in Health and Safety Executive, (<https://www.hse.gov.uk/research/rrhtm/rr931.htm>).
- Shen, X.-M., Clearfield, A., 1986. Phase transitions and ion exchange behavior of electrolytically prepared manganese dioxide. *J. Solid State Chem.* 64, 270–282.
- Shetlemore, M.G., Bundy, K.J., 2001. Examination of in vivo influences on bioluminescent microbial assessment of corrosion product toxicity. *Biomaterials* 22, 2215–2228.
- Shi, J., Hedberg, Y., Lundin, M., Odnevall Wallinder, I., Karlsson, H.L., Möller, L., 2012. The hemolytic properties of synthetic nano- and porous- silica particles: the effect of surface properties and the protection by the plasma corona. *Acta Biomater.* 8, 3478–3490.
- Shoeb, M., Kodali, V.K., Farris, B.Y., Bishop, L.M., Meighan, T.G., Salmen, R., Eye, T., Friend, S., Schwegler-Berry, D., Roberts, J.R., 2017a. Oxidative stress, DNA methylation, and telomere length changes in peripheral blood mononuclear cells after pulmonary exposure to metal-rich welding nanoparticles. *NanoImpact* 5, 61–69.
- Shoeb, M., Kodali, V., Farris, B., Bishop, L.M., Meighan, T., Salmen, R., Eye, T., Roberts, J.R., Zeidler-Erdely, P., Erdely, A., 2017b. Evaluation of the molecular mechanisms associated with cytotoxicity and inflammation after pulmonary exposure to different metal-rich welding particles. *Nanotoxicology* 11 (6), 725–736.

- Sjögren, B., Fossum, T., Lindh, T., Weiner, J., 2002. Welding and ischemic heart disease. *Int. J. Occup. Environ. Health* 8, 309–311.
- Sowards, J., Lippold, J., Dickinson, D., Ramirez, A., 2008. Characterization of welding fume from SMAW electrodes-Part I. *Weld. J.* 87, 106.
- Sowards, J., Ramirez, A., Dickinson, D., Lippold, J., 2010. Characterization of welding fume from SMAW electrodes-Part II. *Weld. J.* 89, 82–90.
- Sowards, J.W., 2006. Henry Granjon Prize Competition 2006 Winner, Category D “Human related subjects” Method for Sampling and Characterizing Arc Welding Fume Particles. *Weld. World* 50, 40–54.
- Tandon, R., Payling, R., Chenhall, B., Crisp, P., Ellis, J., Baker, R., 1985. Application of X-ray photoelectron spectroscopy to the analysis of stainless-steel welding aerosols. *Appl. Surf. Sci.* 20, 527–537.
- Taube, F., 2013. Manganese in occupational arc welding fumes—aspects on physicochemical properties, with focus on solubility. *Ann. Occup. Hyg.* 57, 6–25.
- Teterin, Y.A., Ivanov, K.E., Teterin, A.Y., Lebedev, A.M., Utkin, I.O., Vukchevich, L., 1999. Auger and X-ray photoelectron spectroscopy study of the density of oxygen states in bismuth, aluminium, silicon and uranium oxides. *J. Electron. Spectrosc.* 101–103, 401–405.
- VanWinkle, B.A., De Mesy Bentley, K.L., Malecki, J.M., Gunter, K.K., Evans, I.M., Elder, A., Finkelstein, J.N., Oberdörster, G., Gunter, T.E., 2009. Nanoparticle (NP) uptake by type I alveolar epithelial cells and their oxidant stress response. *Nanotoxicology* 3, 307–318.
- Vishnu, B., Sivapirakasam, S., Satpathy, K., Albert, S.K., Chakraborty, G., 2018. Cr⁶⁺ reduction in welding fumes by nano composite coatings on stainless steel manual metal arc welding electrodes. *Process Saf. Environ. Prot.* 114, 334–346.
- Wanklyn, B.M., 1969. The flux growth of crystals of some fluorides (AlF₃, CrF₃, NiF₂, KNiF₃, CoF₂ and KCoF₃). *J. Cryst. Growth* 5, 279–283.
- Weaver, R.M., Hochella, M.F., Ilton, E.S., 2002. Dynamic processes occurring at the CrIIIaq-manganite (γ -MnOOH) interface: simultaneous adsorption, microprecipitation, oxidation/reduction, and dissolution. *Geochim. Cosmochim. Acta* 66, 4119–4132.
- Westin, E.M., Schnitzer, R., Ciccomascolo, F., Maderthoner, A., Grönlund, K., Runnsjö, G., 2016. Austenitic stainless steel bismuth-free flux-cored wires for high-temperature applications. *Weld. World* 60, 1147–1158.
- Wiebert, P., Lönn, M., Fremling, K., Feychting, M., Sjögren, B., Nise, G., Kauppinen, T., Plato, N., Gustavsson, P., 2012. Occupational exposure to particles and incidence of acute myocardial infarction and other ischaemic heart disease. *Occup. Environ. Med.* 69, 651–657.
- Wu, W.-C., Wang, S.-L., Tzou, Y.-M., Chen, J.-H., Wang, M.-K., 2007. The adsorption and catalytic transformations of chromium on Mn substituted goethite. *Appl. Catal. B* 75, 272–280.
- Yao, Z.-M., Li, Z.-H., Zhang, Y., 2003. Studies on thermal dehydration of hydrated chromic oxide. *J. Colloid Interfaces Sci.* 266, 382–387.
- Zecchina, A., Coluccia, S., Guglielminotti, E., Ghiotti, G., 1971. Infrared study of surface properties of α -chromia. III. Adsorption of carbon dioxide. *J. Phys. Chem.* 75, 2790–2798.
- Zeidler-Erdelyi, P.C., Erdelyi, A., Antonini, J.M., 2012. Immunotoxicology of arc welding fume: worker and experimental animal studies. *J. Immunotoxicol.* 9, 411–425.
- Zhang, X., Lv, L., Qin, Y., Xu, M., Jia, X., Chen, Z., 2018. Removal of aqueous Cr (VI) by a magnetic biochar derived from *Melia azedarach* wood. *Bioresour. Technol.* 256, 1–10.
- Zhou, Q., Liao, B., Lin, L., Qiu, W., Song, Z., 2018. Adsorption of Cu (II) and Cd (II) from aqueous solutions by ferromanganese binary oxide–biochar composites. *Sci. Total Environ.* 615, 115–122.